LASER & PHOTONICS REVIEWS

www.lpr-journal.org

Toward Nonvolatile Switching in Silicon Photonic Devices

*Jorge Parra, Irene Olivares, Antoine Brimont, and Pablo Sanchis**

Nonvolatile switching is still a missing functionality in current mainstream silicon photonics complementary metal-oxide-semiconductor platforms. Fundamentally, nonvolatile switching stands for the ability to switch between two or more photonic states reversibly without needing additional energy to hold each state. Therefore, such a feature may push one step further the potential of silicon photonics by offering new ways of achieving photonic reconfigurability with ultrasmall energy consumption. Here, a detailed review of current developments that enable nonvolatile switching in silicon photonic waveguide devices is provided. Nonvolatility is successfully demonstrated either based on device engineering or by hybrid integration of silicon waveguides with materials exhibiting unique optical properties. Furthermore, several approaches with high potential for evolving toward a nonvolatile behavior with enhanced performance are also being explored. In most cases, many development steps are still necessary to ensure reliable devices. However, this research field is expected to progress in the coming years boosted by current and emerging applications benefiting from such functionality, such as new paradigms for photonic computing or advanced reconfigurable circuits for programmable photonic systems.

1. Introduction

Driven by the growing market demand, silicon photonic integrated circuits (PICs) have reached an unprecedented degree of maturity.[1] Over the past decade, many photonic innovation ecosystems have emerged mostly in the United States, Europe, and Asia, making cutting edge and photonics technologies within reach of tech companies. Their emergence, sustainability, and growth largely rely on the fabless/foundry model that already proved successful for electronics.[2] As a result, PICs with ever-increasing complexity can be now fabricated in well-established low-to-high volume silicon microelectronics foundries using mature complementary metal-oxide-semiconductor (CMOS) compatible processes.[3] Each foundry holds a unique process design kit (PDK) encompassing standard and more advanced photonic building blocks. Despite a focused 20-year-long research and development effort, which has allowed high-performance silicon photonic building blocks to become fully mature and commercially available, nonvolatile functionalities are still missing from standard libraries.[4]

An ideal PIC augmented with nonvolatile capabilities would encompass an interconnected mesh of reconfigurable elements, where switching between stable and reversible photonic states is dynamically achieved using a certain kind of mechanism consuming an ultrasmall amount of energy. Nonvolatility implies that no static energy or holding power is required to retain any of the states once it is set. This ultralow energy consumption coupled with an optimal switching performance opens up a wealth of possibilities wherever highly scalable nonvolatile switching solutions would suppose a significant added value. In fact, owing to the fast spread of photonics in many fields, access to nonvolatile functions is expected to become of high importance in countless current and emerging applications requiring energy efficiency and full reconfigurability, namely, programmable integrated photonic,[5] power-efficient switching in data centers,[6,7] photonic memories,[8,9] neural networks,[10] or large-scale photonic phased arrays for light detection and ranging (LIDAR) systems,[11–13] just to name a few.

Optical bistable performance is a necessary condition to build nonvolatile photonic devices. Here, we focus on bistability based on a looped hysteretic response or latching operation that acts on the effective index of a photonic waveguide structure and allows to retain two (bistable) or more (multilevel) states in a nonvolatile way. **Figure 1** describes the fundamental performance of a generic nonvolatile photonic switching element. The variation of the effective index, which can have a complex nature ($n_{\text{eff}} + j\kappa_{\text{eff}}$), yields to a control of the optical phase and absorption in a separate or coupled scheme depending on the underlying mechanism. Such control can be driven by an electrical or optical excitation for enabling nonvolatile phase or intensity actuators. The optical switching performance can be assessed by different metrics. On one hand, for phase actuators, a large variation in the real part of the effective refractive index (Δn_{eff}) is desired together with low losses and the smallest

J. Parra, I. Olivares, Dr. A. Brimont, Prof. P. Sanchis
Nanophotonics Technology Center
Universitat Politècnica de València
Camino de Vera s/n, Valencia 46022, Spain
E-mail: pabsanki@ntc.upv.es

The ORCID identification number(s) for the author(s) of this article can be found under https://doi.org/10.1002/lpor.202000501

DOI: 10.1002/lpor.202000501

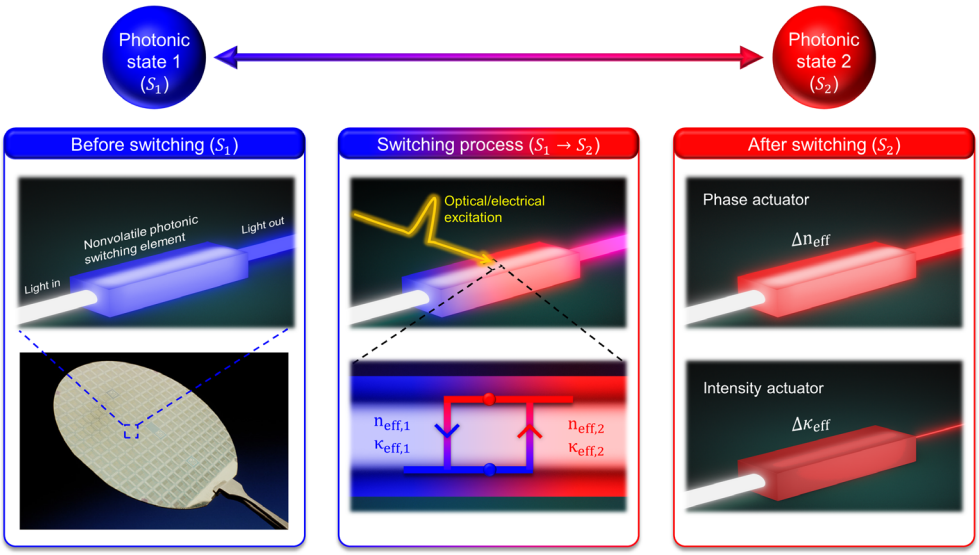

Figure 1. Description of the fundamental performance of a generic nonvolatile photonic switching element. Optical bistable performance is achieved by means of a looped hysteretic response that acts on the effective index of a silicon-based waveguide structure under optical or electrical excitation. The variation of the effective index, which can have a complex nature ($n_{eff} + j\kappa_{eff}$), yields to a control of the optical phase and absorption in a separate or coupled scheme depending on the underlying mechanism. Thereby, nonvolatile switching between two (S_1 or S_2) or more photonic states is enabled.

variation of the imaginary part between photonic states ($\Delta k_{eff} \approx 0$). On the other hand, large variations of the imaginary part (Δk_{eff}) with minimum losses (minimum k_{eff} for S_1 or S_2 in Figure 1) are desired for intensity actuators. Such metrics will determine the insertion loss and extinction ratio of the nonvolatile device. However, it should not be forgotten about other metrics such as energy consumption, switching speed, retention time, footprint, or integration issues. Ideally, the perfect nonvolatile device would maximize all the metrics. In practice, there exist trade-offs among them, and the most suitable nonvolatile approach will be chosen by weighting such metrics. Thereby, a photonic device with access to nonvolatile switching functions should be engineering to fulfill the requirements of a specific application.

In this review, we propose to analyze and compare the existing solutions for nonvolatile switching that might be integrated on the silicon photonics platform. The simplest way to achieve optical bistability on silicon is by exploiting its refractive index variation under a high optical power excitation combined with a photonic structure that provides optical feedback. However, the bistable response is volatile, even though the holding power may be strongly reduced. Therefore, two main strategies are currently followed for providing nonvolatility in silicon photonics devices. On one hand, nonvolatile switching can be enabled by device engineering. The natural approach is staying within the realm of electronic memory-like device engineering in which nonvolatile switching appears as a result of controlled dynamics of charge carriers or taking profit from the resistive switching effect. However, micromechanical systems (MEMS), which take advantage of the electrostatic and mechanical forces at the nanoscale to move and displace photonic waveguide structures, have become a promising alternative with quick progress in the last years. The second main strategy for nonvolatile switching is the hybrid integration of materials with unique optical properties on silicon waveguide structures. In particular, desirable materials are those in which the refractive index can be changed between two or more stable values reversibly. Chalcogenides, mainly germanium-antimony-tellurides, are the most mature candidates due to their intrinsically nonvolatile response at room temperature. However, vanadium dioxide (VO_2) also deserves consideration because, despite its bistable response is shifted from room temperature at regular conditions, the possibility of a nonvolatile switching performance is still in the spotlight. On the other hand, ferroelectrics materials are emerging due to their unique ultrafast and ultralow energy electro-optical response. Finally, the use of liquids with different refractive index changes has also been proposed and demonstrated.

The paper is structured as follows: the mechanisms for inducing optical bistability on silicon are initially described. Then, the proposed approaches for enabling nonvolatile switching based either on device engineering or material integration are thoroughly reviewed. The review has been mostly focused on experimental results and devices with operation at telecom wavelengths unless otherwise stated. Finally, the reviewed approaches are compared in terms of their strengths and weaknesses whereas their perspective for fueling the entrance of nonvolatility in the silicon platform is discussed.

2. Optical Bistability on Silicon

Optical bistability can be achieved by combining an intensity-dependent refractive index change with a photonic structure, such as a ring resonator, providing optical feedback. The mechanisms for changing the refractive index have been based on the thermo-optic and plasma dispersion effects induced by optical absorption. Nonvolatility cannot be achieved using those approaches. However, very low holding powers have been

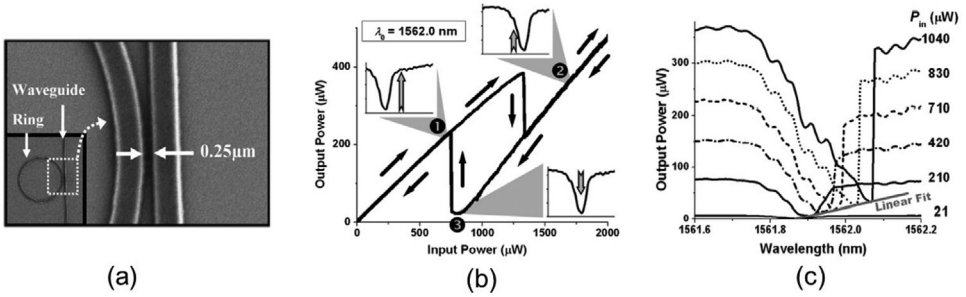

Figure 2. a) Silicon microring resonator used for demonstrating optical bistability. b) Hysteresis curve of output optical power as a function of the input optical power injected into the microring resonator. c) Influence of the optical bistability on the transmission spectrum of the ring resonance when the input power is increased (wavelength is shifted from low to high) Reproduced with permission.[14] Copyright 2004, The Optical Society.

demonstrated by taking profit from the large refractive index of silicon and engineering photonic waveguide structures with high optical field confinement.

2.1. Thermo-Optic Effect

Optical bistability was first proven in silicon devices by using a microring resonator.[14] The microring resonator is shown in **Figure 2**a. The bistable performance arises from the combined effect of the resonance wavelength shift when the input optical power increases and the dependence of the output power on the signal wavelength with respect to the resonance. Figure 2b shows the resulting hysteresis in the output versus input optical power response. Nonvolatility is not achieved so that holding power is always required for exploiting the bistability. Furthermore, the hysteresis curve is highly dependent on the input wavelength that could be an issue for implementing practical devices. On the other hand, the bistable performance may be also observed in the asymmetry and abrupt change in one of the edges of the ring resonance when the input signal is wavelength scanned, as it is shown in Figure 2c. Such effects are accentuated when the input optical power increases.

The resonance wavelength shift is driven by thermal effects induced by optical absorption. The absorbed light is transformed into thermal energy that changes the refractive index of the silicon via its thermo-optic coefficient. Optical absorption may be originated from linear and nonlinear contributions. The role of the different contributions will depend on the photonic structure, waveguide geometry, and fabrication process.[15–17] Linear optical losses are attributed to surface state absorption, which gets stronger in unpassivated waveguides. Optical bistability driven by predominantly linear losses was demonstrated with a holding power of 800 μW, switching energies above 400 pJ, and switching times in the microsecond range.[14] On the other hand, the nonlinear absorption contributions arise from two-photon absorption (TPA) and the associated free carrier absorption (FCA). Optical bistability driven by nonlinear optical losses was achieved in an ultracompact photonic crystal featuring holding powers as low as 40 μW, switching energies in the order of picojoules, and switching times of hundreds of nanoseconds.[18] The energy consumption is significantly reduced owing to the high-quality factor and small mode volume of the cavity. The small size of the cavity also minimizes the switching time. However, the speed is ultimately limited by the slow response associated with thermal effects.

2.2. Plasma Dispersion Effect

Optical bistability based on carrier effects induced by TPA has been proposed to reduce the switching time in comparison with thermal-based approaches. In this case, the refractive index of silicon decreases as the input power is increased due to the plasma dispersion effect. Switching times in the nanosecond range have been demonstrated by using a microring resonator but at expense of high holding power of around 5.5 mW and high insertion losses up to 12 dB.[19] On the other hand, thermal effects induced by optical absorption cannot be generally neglected. Therefore, the variation of the silicon refractive index is influenced by two opposite effects that degrade the bistable performance and, in particular, the stability of the high-power state. The influence of thermal effects has been minimized by modifying the fabrication process for achieving ultrasmooth Si/SiO_2 interfaces.[20] However, the carrier lifetime is also increased which gives rise to longer switching times. Ultrahigh quality nanocavities based on a photonic crystal structure have also been employed for reducing the switching energy.[21] Despite a more critical narrowband operation, the high optical confinement allowed to drastically reduce the switching energy down to 100–200 fJ and the holding power to values between 1.6 and 7.9 μW.[22] On the other hand, the plasma dispersion effect can also be exploited by using more efficient p-i-n junctions integrated into the silicon waveguide. In this case, even lower switching energies down to a few femtoseconds and speeds up to 20 GHz have been predicted.[23] Nevertheless, it should be noted that, in all cases, the optical switching performance is volatile and highly wavelength-dependent because photonic cavities are required to provide optical feedback.

3. Nonvolatile Switching Enabled by Device Engineering

Optical switching with a nonvolatile response can stem from device engineering without the need of optical feedback. The main approaches rely on the adoption of electronic nonvolatile configurations, such as flash memories or resistive switching devices, or novel switching devices driven by MEMS actuators.

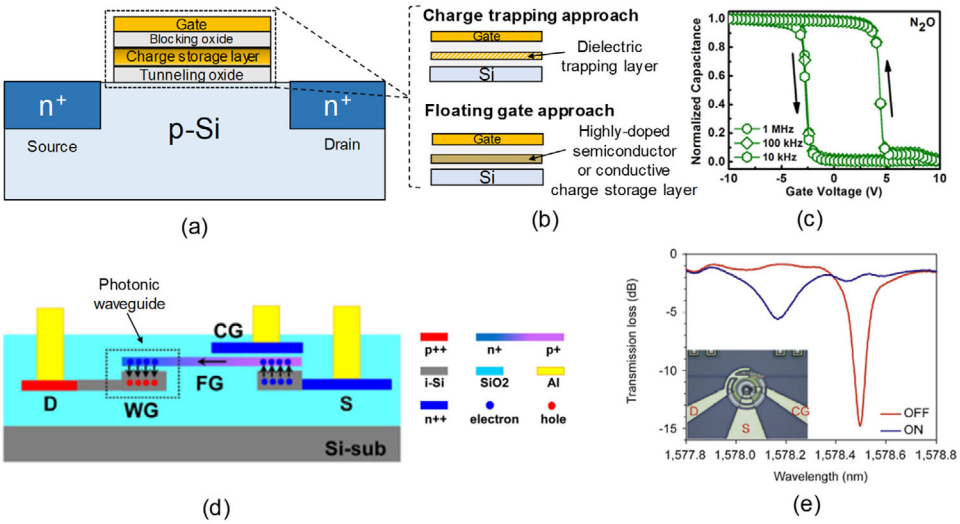

Figure 3. a) General scheme of an electronic nonvolatile flash memory. b) Detailed view of charge trapping (top) and floating gate (bottom) approaches. c) Capacitance–voltage curves of a flash memory device in the frequency range of 10 kHz to 1 MHz. The hysteresis is due to the trapped charges in the stored layer. Reproduced under the terms of a CC-BY 4.0 license.[24] Copyright 2017, The Authors. Published by Springer Nature. d) Photonic waveguide structure based on a floating gate approach and e) experimental nonvolatile change of the optical response in a microring resonator. Reproduced under the terms of a CC-BY 4.0 license.[25] Copyright 2016, The Authors. Published by Springer Nature.

3.1. Mimicking Electronic Memories

Microelectronics provides not only tools for fabricating PICs but also knowledge regarding nonvolatile devices. One of the most natural approaches to provide nonvolatility to photonic integrated waveguides is the adaptation of the well-known and proved flash memory cell. In this case, the waveguide is combined with different CMOS-compatible materials such as oxides, doped-semiconductors, and metals. Therefore, such devices would come with the main advantage of maximum CMOS compatibility together with a nonvolatile behavior. A bistable response at room temperature arises by using a metal-oxide-silicon (MOS) structure in which the gate oxide is replaced by a three-layer stack. The stack comprises a charge storage layer sandwiched between a tunneling and blocking oxide. The concept is schematically illustrated in **Figure 3**a. Depending on the nature of the middle layer, the structure may be classified into two groups: floating-gate and charge trapping devices. Both approaches rely on the injection of carriers via the tunneling effect from the silicon substrate. While in a floating gate scheme the charge is stored in a conductor or a heavily doped semiconductor, charge trapping devices use a dielectric layer, such as silicon nitride, to retain the injected carriers, as shown in Figure 3b.

The increase in the flatband voltage owing to the trapped charges is taken advantage of to obtain nonvolatility. Thereby, a counter-clockwise hysteresis is obtained when performing capacitance–voltage measurements, as depicted in Figure 3c. For positive voltages, charges are injected from silicon to the storage layer whereas, for negative voltages, carriers are tunneled back to the substrate. There are three main physical effects used to inject carriers through the tunneling oxide: i) direct and ii) Fowler-Nordheim tunneling, and iii) hot carrier injection. While the first two do not require the source and drain electrode to inject carriers, for hot carrier injection an applied voltage is needed to make the electrons gain kinetic energy through the channel. When they have enough energy to jump the oxide barrier, they are injected into the charge store layer thanks to the vertical field created by the gate voltage. Finally, for charge trapping devices, the Poole-Frenkel effect trap-assisted tunneling should be considered when modeling the current and carrier distribution across the trapping layer.

One of the main differences between floating gate and charge trapping schemes is found in their reliability. Owing to the conducting nature of the floating gate, a single defect in the thin tunnel oxide causes the complete discharge of the device. This issue is avoided in charge trapping devices, thus allowing for thinner tunnel oxides and lower programming and erasing voltages. On the other hand, longer retention periods are easier to achieve in floating gate structures owing to their larger detrapping barrier height. In general, a balance must be established among speed, oxide thickness, and charge retention.

3.1.1. Plasma Dispersion Effect

The integration of the flash memory with silicon photonics has been mainly done by placing the charge store layer as near as possible to the waveguide structure.[25–28] The optical phase is then changed by means of the plasma dispersion effect owing to the overlap of the guided mode either with the trapped carriers or with the screened charge inside the silicon waveguide. An additional interferometric or resonant photonic structure is required to transform the optical phase change into an optical intensity variation. The first photonic device following the flash memory approach was proposed in 2006 by integrating a charge trapping structure based on silicon nitride into a silicon microring.[26] However, only simulations were provided. The carrier injection process was carried out with voltages below 10 V. One of the constraints of this configuration is the proximity of the metal control

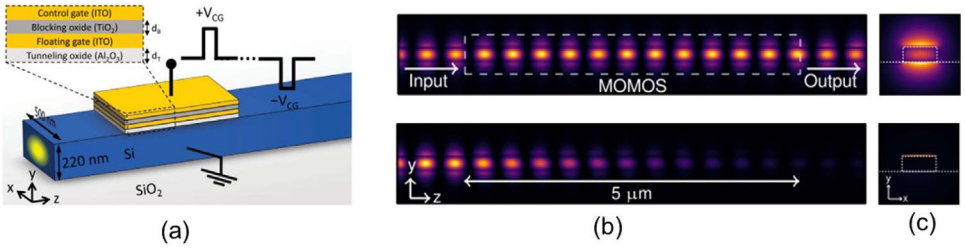

Figure 4. a) Nonvolatile optical switch based on exploiting ITO unique properties in a floating gate approach. b) Simulated optical switching performance for the two states with low/high optical losses in the so-called metal-oxide-metal-oxide-semiconductor (MOMOS) waveguide. c) Optical mode at each switching state. Reproduced with permission.[32] Copyright 2019, The Optical Society.

gate to the guiding structure. A thick blocking oxide is needed to avoid excessive optical losses and, consequently, around 100 V is needed to discharge the device. A similar approach has been experimentally demonstrated for trimming purposes.[27] In this case, the carrier injection from the silicon substrate was aided by exposing the device to ultraviolet light. More recently, a new configuration based on using hafnium oxide as trapping layer has also been proposed by means of simulations to reduce the switching time to around 100 μs with gate voltages between 20 and 30 V.[29]

A nonvolatile performance has also been demonstrated by using the floating gate approach.[25,28] The cross section of the proposed waveguide structure is depicted in Figure 3d. During the charging process, the carriers are injected into the floating gate using a typical floating gate memory structure. Once injected, those carriers redistribute inside the charge storage layer and change the effective refractive index of the guided mode via the plasma dispersion effect. A microring structure was also used to transform the optical phase change into an optical intensity variation. Figure 3e shows the experimental nonvolatile change of the microring optical response. The transition between the uncharged and charged state is achieved in the millisecond range with a gate voltage of 20 V demonstrating, in addition, a multilevel operation for intermediate injection times.

3.1.2. Integrating Advanced Materials

Recently, several works have also investigated through simulations of the use of graphene and transparent conducting oxides (TCOs), such as indium tin oxide (ITO) or cadmium oxide (CdO), as materials for the floating gate in flash memory structures. Despite graphene exhibits stronger free carrier dispersion than silicon, the weak interaction of the optical mode with the atomically thin material results in still large footprint devices. Phase actuators with a length of around 650 μm for a π phase shift together with ≈3 dB of loss, and intensity actuators with around 330 μm of length to attenuate 20 dB, have been reported.[30] However, the length could be drastically reduced by replacing graphene with TCOs. In that regard, TCOs exhibit a large free carrier dispersion effect that is combined with a strong light–matter interaction owing to the epsilon-near-zero (ENZ) regime.[31] Therefore, broadband and ultracompact nonvolatile devices have been prospected. A 5-μm-long intensity device has been proposed using ITO.[32] The device is shown in **Figure 4**a. Extinction ratios greater than 10 dB in a bandwidth of 100 nm were reported. Such values were enabled by the increase of optical absorption in the ITO with carriers together with the ultrahigh confinement of the optical mode within the ITO floating gate owing to the ENZ regime. The simulated optical switching performance is shown in Figure 4b, whereas the optical modes at each state are depicted in Figure 4c. Interestingly, this difference in the shape between the typical photonic mode and the ENZ mode was also exploited for nonvolatile switching by integrating the nonvolatile waveguide in a directional coupler.[33] On the other hand, phase shifters could be attained by using high-mobility TCOs instead of ITO to reduce the loss while maintaining a large change on the real part of the effective index. By replacing ITO with CdO, a π phase shift could be obtained in 30 μm with an optical loss of around 1 dB.[34] Yet, the main pending challenge is the experimental demonstration of all these proposed devices.

3.2. Resistive Switching Devices

Resistive switching has been largely investigated for enabling resistive random access memories (RRAMs) based on the bistable behavior present in the electric response.[35,36] Basically, the electrical resistance is changed between a low and high resistive state following a pinched current–voltage hysteresis loop. Here, we focus on resistive switching based on the formation and destruction of conductive nanofilaments across an active material sandwiched between two electrodes.[37,38] For photonic applications, the resistance change may give rise to a variation of the optical losses with also a hysteretic response.[39] However, the optical switching performance will depend not only on the active material but also on the surrounding materials and device structure.

3.2.1. Resistive Switching with Amorphous Silicon

The resistive switching effect was first demonstrated in hybrid plasmonic waveguides by using amorphous silicon as active material.[40] **Figure 5**a shows the hybrid plasmonic waveguide. Plasmonic waveguides allow high optical mode confinement on the ultrathin active layer, as is depicted in Figure 5b. Metal filaments are formed in the amorphous silicon layer by silver ions injected from the top silver electrode when a positive voltage is applied. The formation of metal filaments increases optical losses. The associated optical transmission variation is depicted

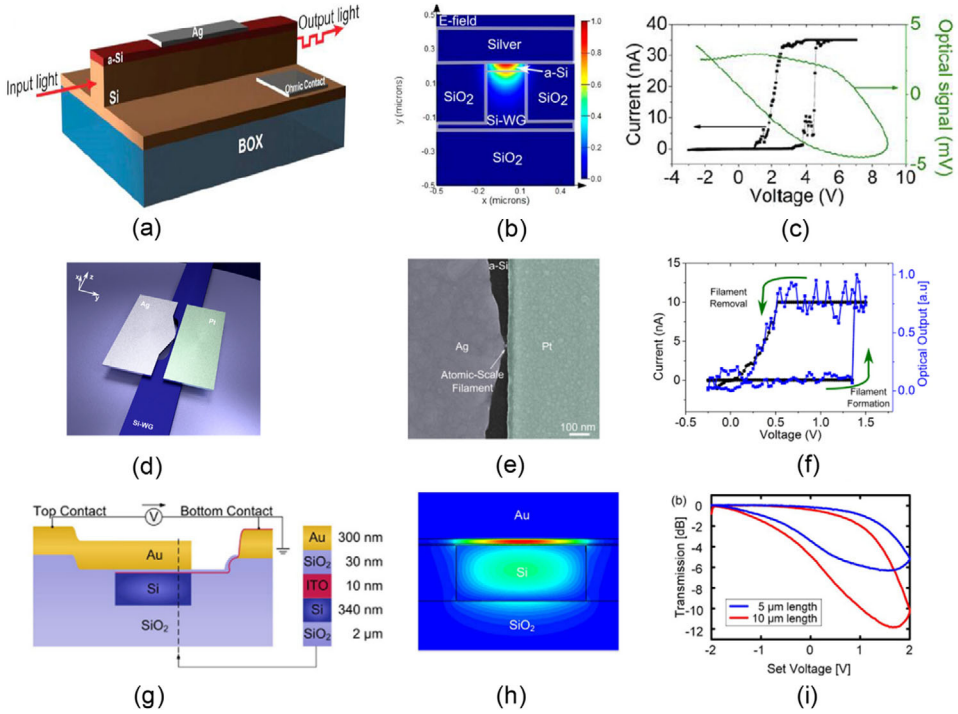

Figure 5. a) Nonvolatile optical switching based on resistive switching in amorphous silicon: hybrid plasmonic waveguide device, b) optical mode showing the light confinement at the amorphous silicon layer, and c) measured electrical and optical switching performance. Reproduced with permission.[40] Copyright 2013, American Chemical Society. d) Plasmonic device based on resistive switching on amorphous silicon at an atomic scale, e) SEM image of the fabricated device and f) measured optical switching response. Reproduced with permission.[41] Copyright 2015, American Chemical Society. g) Hybrid plasmonic waveguide for nonvolatile optical switching based on resistive switching in silica, h) simulated optical mode, and i) measured optical switching response for two different waveguide lengths. Reproduced with permission.[42] Copyright 2014, The Optical Society.

in Figure 5c. The maximum extinction ratio is not achieved at 0 V which penalizes the nonvolatile performance. Such behavior is because the bistability of the electrical switching is usually shifted at positive voltages, as can also be seen in Figure 5c. Nevertheless, a switching power as low as 0.15 μW is achieved. On the other hand, the insertion loss is around 4.2 dB. The propagation losses of the plasmonic waveguide and the coupling losses to the connecting silicon waveguides need both to be considered for minimizing insertion losses.

Resistive switching in amorphous silicon has also been exploited for optical bistable switching at an atomic scale.[41] The device is shown in Figure 5d,e. The active region is driven as a plasmonic nanocavity in which a single nanofilament is created or erased. The resulting optical bistable response is shown in Figure 5f. Nonvolatility switching is not achieved, but the ultrasmall scale of the active region allows reducing the holding power to a few nanowatts and achieving switching energies as low as 12.5 fJ. However, the switching bandwidth is limited to 1 MHz. Further work is also required to investigate the influence of quantum effects on the optical switching mechanism.

3.2.2. Resistive Switching with Silicon Dioxide

Resistive switching has also been demonstrated in hybrid plasmonic waveguides with silicon dioxide as active material.[42] Figure 5g shows the waveguide cross section which is based on a layer stack made of gold, silicon dioxide, and ITO on top of the silicon waveguide. The optical mode is depicted in Figure 5h. The photonic structure was initially intended for carrier modulating in the ITO layer. Instead, a nonvolatile optical switching performance was achieved owing to a resistive switching effect in the silica layer. The silica layer was deposited by RF sputtering which is expected to originate a high number of defects. Metal filaments are formed in the silica by ions injected from the top gold electrode. The formation of filaments is expected to be facilitated by a large number of defects in the silica. Figure 5i depicts the optical transmission as a function of the applied electrical voltage for different lengths of the plasmonic waveguide. Nonvolatile switching with an extinction ratio of around 5 dB and a switching power of 200 nW was achieved. However, a dependency of the extinction ratio with the duration of the applied electrical pulses was found when studying the dynamic performance. Thereby, the switching energy was between 60 μJ and 1 nJ depending on the switching duration. Furthermore, a frequency response of 30 MHz and high insertion losses above 10 dB were reported.

3.2.3. Resistive Switching with Other Materials

The resistive switching effect has also been proved in a large variety of materials and layer stacks that could give rise to new approaches for nonvolatile optical switching. However, there is not yet a clear material candidate and there are still challenges for

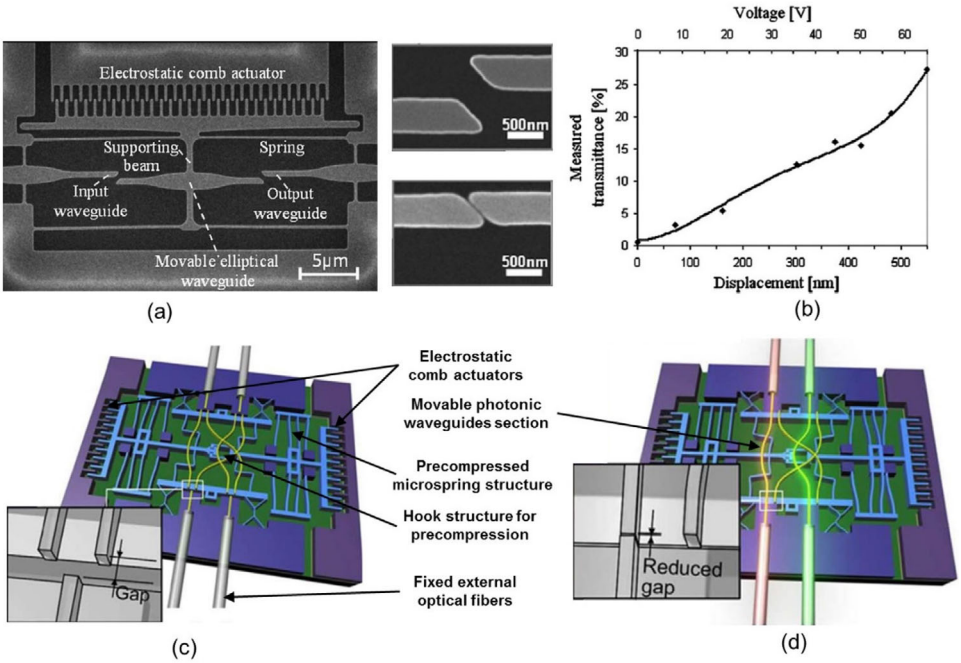

Figure 6. a) SEM image of optical switch driven by an electrostatic comb actuator. Optical switching with volatile performance is based on the displacement of a central movable waveguide with respect to the input/output fixed waveguides, as shown in the two smaller SEM images at the right. b) Measured optical transmittance as a function of the applied voltage and induced displacement. Reproduced with permission.[52] Copyright 2008, AIP Publishing. c) Nonvolatile optical switch based on a precompressed microspring structure driven by two electrostatic comb actuators. d) The central movable photonic waveguide section is moved to the right position after the precompressed microspring structure is switched. The insets show that there is a gap between the movable and fixed sections during the movement that is minimized when the switching process has finished. Adapted with permission.[53] Copyright 2009, IEEE.

developing reliable devices.[38] For photonics, oxide compounds such as HfO_2,[43] TiO_2,[44] ZnO,[45] or silicon-rich oxides[46,47] could be good alternatives owing to their low optical losses at telecom wavelength and CMOS compatibility. Electrical memory devices may be built in a relatively easy way as they basically rely on a simple layer stack. However, the integration in silicon photonic waveguide devices remains an open challenge. On the other hand, a good understanding and control of the underlying physics are also of paramount importance. The formation and destruction of the conductive nanofilaments have been mainly attributed to electrochemical metallization, valence change, and thermochemical mechanisms. However, the most suitable mechanism or combination of mechanisms for optical switching and their influence on the device performance is still unclear.[48] Electrochemical metallization is based on the diffusion from ions of a metal electrode, and it has been the mechanism used in photonic waveguide devices featuring resistive switching. The valence change mechanism usually dominates on materials with oxygen-related defects. Conductive filaments are formed by oxygen vacancies induced by ions migration. Electro-optical switching has been demonstrated with ZnO in the mid- and large infrared (from 5 to 18 μm) but on a simple layer stack device.[49] Concerning the last mechanism, thermochemical reactions and Joule heating dominate the forming and destruction of the filaments. In this case, unipolar switching is more effective but the influence of the thermal processes on the device speed would need to be carefully analyzed. Furthermore, electro-optical switching has not been demonstrated to the best of our knowledge.

3.3. Silicon MEMS Devices

The integration of MEMS in photonic devices for enabling novel designs of tunable components has emerged as a very promising field in the past years.[50,51] Tunability is achieved by a mechanical actuation mechanism that changes the optical properties of a photonic waveguide or structure. One of the simplest ways for achieving optical switching is by a lateral displacement of a movable photonic waveguide in between two fixed waveguides, as can be seen in **Figure 6**a.[52] The movable waveguide is suspended in air and driven by an electrostatic comb actuator, but the optical switching performance is volatile. The waveguide is moved by the electrostatic force induced by the actuation voltage, whereas the original position is restored when the voltage is no longer applied owing to the resulting spring force originated in the suspended structure. Figure 6b shows the measured optical transmittance as a function of the applied voltage and induced lateral displacement. An experimental extinction ratio of 15 dB was achieved for a displacement of 540 nm using 65 V. The measured switching time was around 10 μs. Despite the high actuation voltages required, the switching energy consumption is low owing to the capacitive operation of the electrostatic actuator.

Nonvolatile optical switching can be achieved by modifying the MEMS actuator for enabling a nonvolatile bistable movement. This has been experimentally demonstrated by using a precompressed microspring structure that can be switched between two stable positions.[53] The switching device is shown in

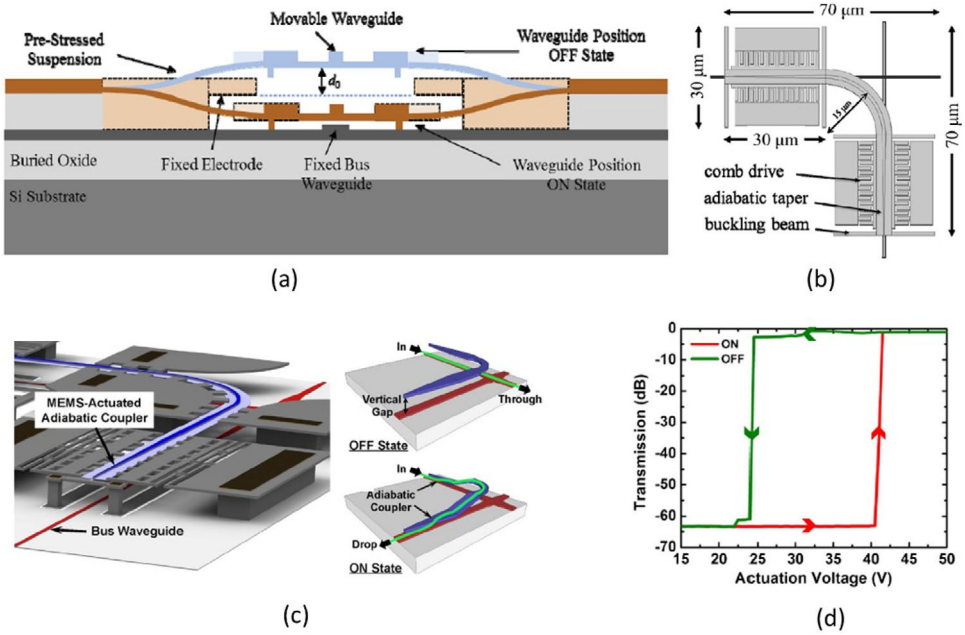

Figure 7. a) Cross section of coupler structure proposed for nonvolatile optical switching performance with movable waveguides in the vertical direction driven by b) two vertical comb electrostatic actuators. Reproduced with permission.[54] Copyright 2019, SPIE. c) Silicon switch based on the same coupler structure but driven by a volatile bistable actuator. d) Measured optical transmission response as a function of the actuation voltage. Reproduced with permission.[55] Copyright 2016, The Optical Society.

Figure 6c. The precompression is only obtained after fabrication by locking a hook structure located at the center of the device. The nonvolatile optical switching performance is obtained by a lateral displacement of the central movable photonic waveguide section by switching between the precompressed states of the microspring structure by means of the electrostatic comb actuators, as depicted in Figure 6d. A switching voltage above 36 V was required while the measured switching time was around 0.5 ms. On the other hand, insertion losses of 3 dB of the whole assembly, including fiber-to-waveguide coupling losses, were reported.

A similar concept has been proposed for enabling a nonvolatile optical switching performance but on a silicon coupler structure with movable waveguides in the vertical direction.[54] The cross section of the coupler structure is shown in **Figure 7**a. The movable waveguide is fabricated in an additional suspended polysilicon layer with residual compressive stress. Thereby, two mechanical stable states can be achieved by taking advantage of such precompressed stress and proper design of the geometry of the suspended structure. The movement is driven by two vertical comb electrostatic actuators, as depicted in Figure 7b, which generate the required electrostatic force to exceed the critical bending force of the movable waveguide structure.

A full demonstration of nonvolatile optical switching has not yet been reported and only the mechanical parts have been designed and experimentally characterized. However, the optical switching performance of the vertical coupler structure has been demonstrated in previous devices.[55] The switch device and principle of operation are depicted in Figure 7c. In this case, the electrostatic actuator was based on a parallel-plate arrangement with volatile performance. Thereby, the movable waveguide is pulled down to the fixed bus waveguide when the voltage is applied to the actuator. The optical transmission response as a function of the actuation voltage is shown in Figure 7d. It can be seen that the optical switching performance is volatile. However, an optical bistable operation is achieved owing to the nonlinear behavior of the electrostatic force applied by the actuator. Insertion losses as low as 0.47 dB and ultralarge extinction ratios above 60 dB were demonstrated. Furthermore, switching times down to 300 ns and switching operations over 10 billion cycles were also reported. One of the main challenges is that the fabrication requires additional process steps for enabling the suspended waveguide structures and MEMS actuators, which require tighter control and increase the complexity of the overall manufacturing. However, their potential for large-scale integration has been proved with success. Recently, a large switching matrix with 240 × 240 elements and maximum insertion losses below 10 dB has been demonstrated.[56]

4. Nonvolatile Switching Enabled by Materials Integration

The integration of materials with a refractive index that can be switched between bistable states upon an external excitation represents another promising strategy for enabling a nonvolatile optical switching performance on silicon waveguide devices.

4.1. Chalcogenide Compounds

Chalcogenide compounds are currently used in the development of nonvolatile memories for removable optical data storage such

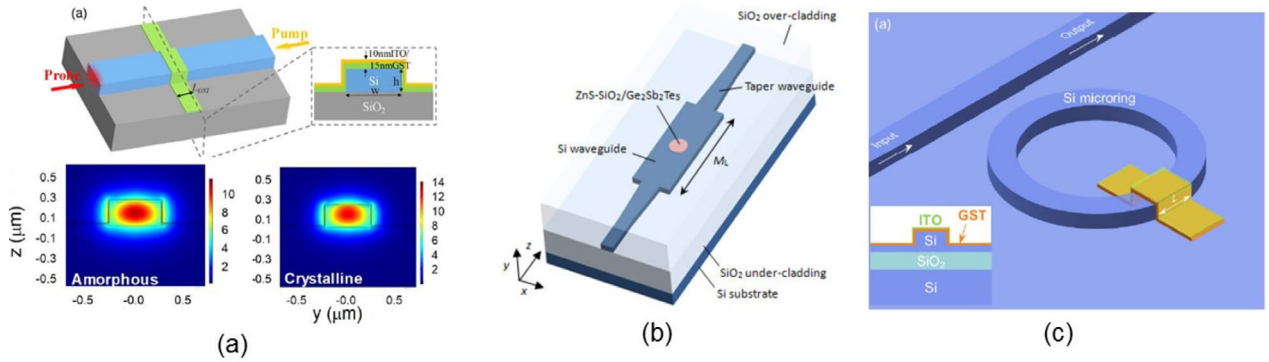

Figure 8. a) Hybrid GST/Si waveguide optically activated with an in-plane optical pumping. Reproduced with permission.[65] Copyright 2018, The Optical Society. b) Hybrid device based on a silicon multimode interference to reduce insertion losses and increase switching speed. Reproduced with permission.[66] Copyright 2012, The Optical Society. c) Hybrid ring resonator to increase extinction ratio and reduce energy consumption. Reproduced with permission.[67] Copyright 2018, The Optical Society. Nonvolatile optical switching in (b) and (c) was triggered with an out-of-plane optical pumping.

as rewritable DVDs.[57] The main benefits are the possibility of enabling simple memory cells with small energy consumption, long data retention, and multilevel storage capability. However, the use for photonic applications has only been recently addressed.[58–60] Until now, the most promising results have been achieved by using germanium-antimony-tellurides and, in particular, $Ge_2Sb_2Te_5$, usually named GST.[61] The material can be switched between an amorphous and crystalline state in a reversible and nonvolatile way. The refractive index is drastically changed between the two states with possible intermediate values by partial crystallization. A refractive index of $4.69 + j0.19$ (amorphous) and $8.03 + j1.88$ (crystalline) has been reported at 1.55 μm.[62] Thereby, ultracompact devices may be accomplished that makes GST one of the most attractive candidates for enabling nonvolatile silicon photonic devices with a multilevel operation. However, it should be highlighted that, while maintaining the large variation between both states, different refractive index values can be found in the literature.[63] Therefore, ideally, the refractive indices should be measured for an optimal device design because they can vary significantly owing to fabrication and deposition processes.[64]

Hybrid GST/Si waveguides can be simply made by depositing a small thin layer of GST on top of the silicon waveguide as depicted in **Figure 8**a. The GST layer must be covered to avoid oxidation from the air as the phase state is triggered by heat. On one hand, the crystalline state is achieved by heating the material above the crystallization temperature (≈160 °C), typically with values around 180–250 °C. On the other hand, the material needs to be heated above the melting temperature (≈600 °C) and then quenched by rapid cooling (≈ns) for amorphization. The reach of such high temperature increases the energy consumption. On the other hand, the switching time between states is generally slower for crystallization and physically limited to hundreds of picoseconds.[68] However, the operation speed will depend on the excitation used for driving the thermally mediated phase change and the influence of the generated heat on the photonic structure.[63] Optical pumping has been the dominant approach until now for analyzing the nonvolatile switching performance in hybrid waveguide devices. Out-of-plane optical pumping was used in the first demonstration of a hybrid GST/Si waveguide device.[69] The switching speed and insertion losses were further improved by designing a silicon multimode interference waveguide, shown in Figure 8b, with optical light concentrated on a 1 μm-diameter circular-shaped GST film deposited on top.[66] Hybrid GST/Si waveguides with a few micrometer lengths and GST thicknesses of 20 nm have also been integrated on silicon ring resonators, as depicted in Figure 8c, for achieving extinction ratios of 12 dB[70] and even larger than 30 dB.[67] However, the switching performance in cavities and multimode structures is influenced by undesired variations of the silicon refractive index owing to heat and free carriers, which may also be induced by the strong optical absorption.[66,70]

On the other hand, in-plane optical pumping was first demonstrated with SiN waveguides, as shown in **Figure 9**a. Optical pulses with switching energies of 533 pJ were required to achieve an optical contrast of 21% in a 5 μm-long hybrid waveguide.[72] However, nonuniform heating of the GST layer occurs with an in-plane optical pumping excitation, as also depicted in Figure 9a. Hence, switching to the crystalline state with a single optical pulse is challenging owing to the rapid increase of optical absorption which could lead to reamorphization if the phase transition occurs before the end of the optical pulse.[73] A train of optical pulses with decreasing energy has been proposed to avoid reamorphization of already crystallized regions, as shown in Figure 9b, which could also be exploited for enabling a nonvolatile multistate operation. However, the switching time response and energy consumption will notably increase. More recently, a double-step optical pulse approach, depicted in Figure 9c, has been demonstrated to reduce the energy consumption and increase the overall speed during the crystallization process.[71,74] On the other hand, in-plane optical pumping with hybrid GST/Si waveguides has been only reported in few works.[65,75] A switching energy of ≈1 nJ was required for nonvolatile optical switching on a 2 μm-long hybrid GST/Si waveguide with 5 dB extinction ratio.[65] On the other hand, a switching energy of 9.5 nJ and switching time of 3.8 μs were used to obtain a maximum optical contrast of 12% in a 4 μm-long hybrid GST/Si rib waveguide.[75] In general, higher energy but faster speed is achieved compared with hybrid GST/SiN waveguides owing to the higher thermal conductivity of silicon and lower confinement of the optical mode in the GST layer.

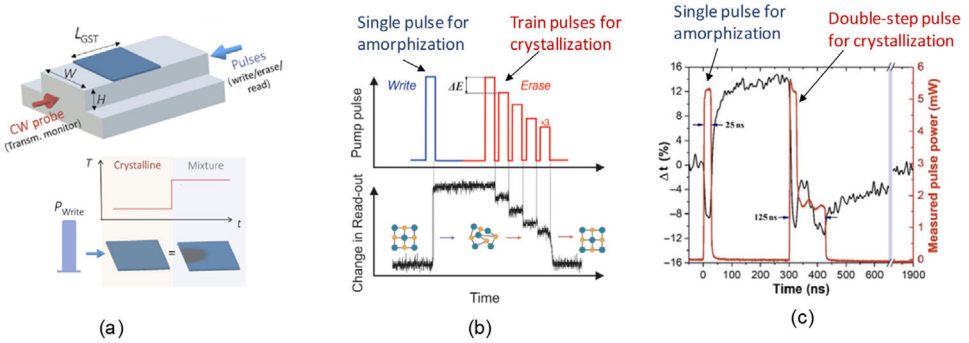

Figure 9. a) Nonvolatile switching with in-plane optical pumping was first demonstrated with SiN waveguides. Nonuniform heating of the GST layer occurs with this kind of excitation. b) Optical pulses for driving the GST phase change. A single optical pulse is sufficient for amorphization while a train of optical pulses with decreasing energy has been proposed for crystallization. Reproduced with permission.[72] Copyright 2015, Springer nature. c) Energy consumption and operation speed were improved by using a double-step optical pulse for crystallization. a,c) Reproduced under the terms of a CC-BY 4.0 license.[71] Copyright 2019, The Authors. Published by AAAS.

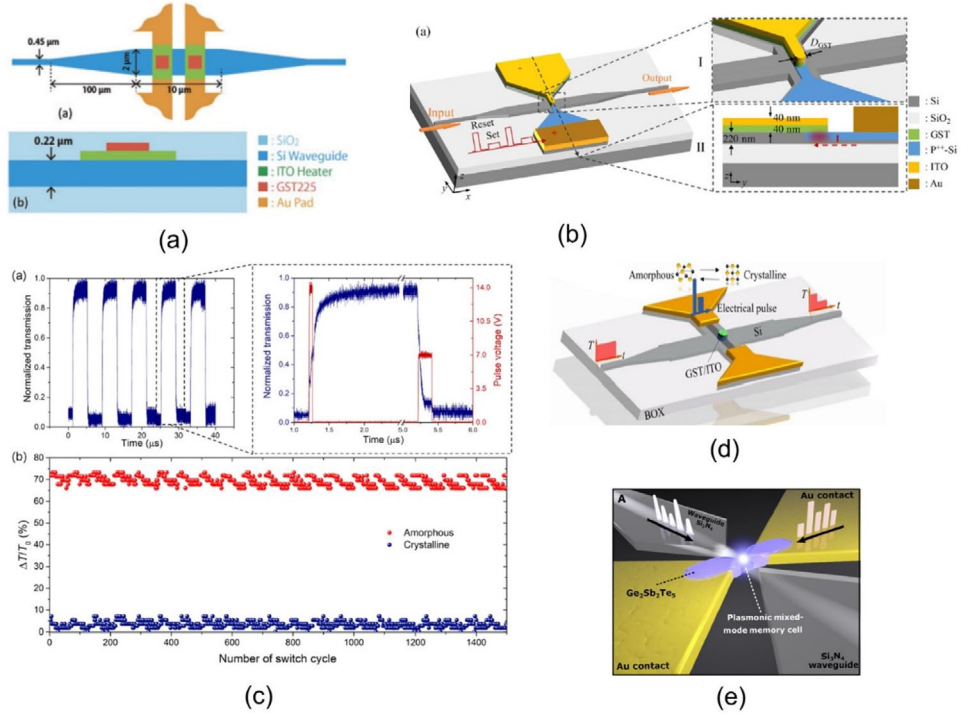

Figure 10. a) Hybrid GST/Si waveguide device electrically activated by means of Joule heating applied with ITO heaters. Reproduced under the terms of a CC-BY 4.0 license.[76] Copyright 2017, The Authors. Published by IOP Publishing. b) Similar device but based on heating the silicon below the GST layer and c) measured nonvolatile optical switching response triggered by single voltage pulses. Reproduced under the terms of a CC-BY 4.0 license.[78] Copyright 2019, The Authors. Published by Elsevier. d) Improved hybrid GST/Si waveguide device to reduce insertion losses. Reproduced with permission.[79] Copyright 2019, American Chemical Society. e) Plasmonic structure for exploiting both the electrical and optical changes in the GST layer and reduce energy consumption. Reproduced under the terms of a CC-BY 4.0 license.[80] Copyright 2019, The Authors. Published by AAAS.

Nonvolatile optical switching has also been electrically demonstrated in a hybrid GST/Si waveguide by means of Joule heating applied with ITO heaters.[76] The use of ITO as a heater allows for reducing optical losses and may reduce power consumption.[77] The hybrid waveguide structure is shown in **Figure 10**a. The GST is placed on top of a silicon wide waveguide. The extinction ratio was only 1.2 dB owing to the small active region and weak interaction with the optical mode. Furthermore, high switching energies of 14.4 and 4.2 mJ for the amorphization and crystallization, respectively, were required. Recently, nonvolatile optical switching in a similar hybrid GST/Si waveguide device has also been demonstrated by means of electrical excitation but heating the silicon below the GST layer.[78] The hybrid GST/Si waveguide structure is shown in Figure 10b. The silicon was highly doped below the GST to optimize the heat transfer process and achieve an ohmic contact with the metallic electrodes but high insertion losses of 7.5 dB were reported owing to a nonamorphization of the whole active region.

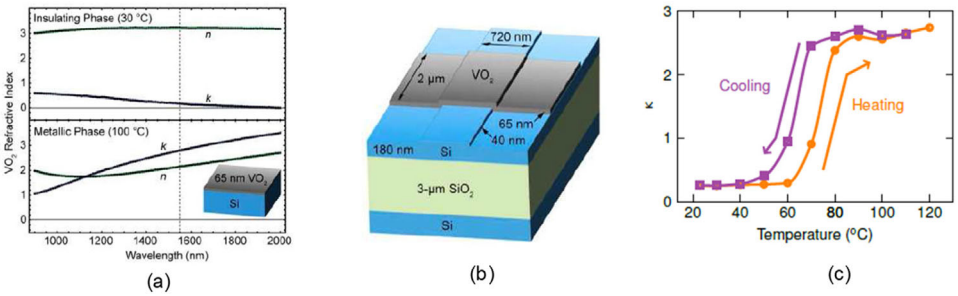

Figure 11. a) VO_2 refractive index at the insulating and metal states for telecom wavelengths and b) typical hybrid VO_2/Si waveguide. Reproduced with permission.[88] Copyright 2010, The Optical Society. c) Hysteretic variation of the imaginary part of the refractive index as a function of temperature at a wavelength of 1550 nm. Reproduced with permission.[93] Copyright 2021, IEEE.

By using electrical excitation, a single voltage pulse could be used for both crystallization and amorphization, as can be seen in Figure 10c. However, as a difference with optical excitation, the amorphization process could be now more critical because an efficient heat dissipation or electrical pulses with fast fall times are required to avoid recrystallization when switching from the crystalline to the amorphous state. In further work, the GST region was optimized with a small circular geometry (Figure 10d) for a more efficient amorphization process thus reducing insertion losses.[79] Furthermore, the influence of parameters such as the electrical pulse duration and voltage and GST size were analyzed. Nonvolatile optical switching and multilevel operation were demonstrated with switching energies of around 10 nJ and switching times above 100 ns. A plasmonic structure, shown in Figure 10e, has also been proposed to exploit both the electrical and optical changes in the GST layer.[80] The stronger light–matter interaction allows to drastically reduce the footprint. The nonvolatile switching performance was characterized by driving the device with both optical and electrical excitations. The switching energy with optical excitation was reduced by a factor of 6 (around tens of pJ) compared to previous works.[72] On the other hand, subvolt voltages were sufficient for electrically driving the GST state. However, in this case, the optical contrast was only around 0.6%.

One challenge of GST is that the optical absorption is relatively high (between 1 and 4 dB μm^{-1}) at the amorphous state, which increases the insertion losses of the final device. A possible solution is to engineer the photonic structure in a clever way. By following this strategy, a 1 × 2 switch with insertion losses lower than 1 dB has been recently demonstrated by patterning and encapsulating the GST into subwavelength structures.[81] Furthermore, the subwavelength patterning allowed GST to be switched more efficiently, i.e., with lower energy consumption, and faster. On the other hand, the use of other GST alloys, such as $Ge_2Sb_2Se_4Te_1$ (GSST)[82–84] or $Ge_2Sb_2Se_5$ (GSS),[85] with smaller optical losses at both phase states in the telecom wavelength range has also been proposed to implement nonvolatile photonic devices with lower insertion losses.

4.2. Vanadium Dioxide

Vanadium dioxide (VO_2) also stands out as a promising material for photonics.[86,87] The key feature of this material is a reversible phase transition between an insulating and metallic state. At telecom wavelengths, the refractive index is drastically changed between both states, as shown in **Figure 11**a. At 1.55 μm, the value changes from 3.21 + *j*0.17 (insulating) to 2.15 + *j*2.79 (metallic).[88] Therefore, ultracompact devices with a broad response can be developed. However, it should be noted that variations of those values are also found in the literature.[89] Similar to GST, the typical hybrid VO_2/Si waveguide is comprised of a standard silicon waveguide with a thin VO_2 layer on top, as illustrated in Figure 11b. The interaction that exists between the optical mode and the VO_2 at both states leads to a change on the effective refractive index that translates in both an optical phase and optical loss variation that can be exploited for optical switching. Ultracompact (<20 μm) VO_2/Si waveguides with large extinction ratios between the insulating and metallic state for TE (≈25 dB) and TM (>40 dB) polarization either using a straight waveguide[90,91] or in a Mach-Zehnder interferometer or microring resonator[92] have been demonstrated. On the other hand, competitive insertion loss below 0.05 dB μm^{-1} for TE polarization and 0.3 dB μm^{-1} for TM polarization has been achieved by engineering the morphology of the VO_2 layer.[90]

The dominant mechanism for triggering the VO_2 phase transition has been temperature. The variation of the imaginary part of the refractive index, or extinction coefficient, as a function of temperature and at a wavelength of 1550 nm is depicted in Figure 11c. The extinction coefficient shows a hysteretic response but centered around 65 °C. Therefore, holding power is required to exploit the bistability induced by the hysteresis loop. However, thermal requirements are more relaxed in contrast with chalcogenides as the phase change occurs near room temperature and is not restricted by a minimum cooling rate. Localized heating on the hybrid VO_2/Si waveguide can be achieved by means of Joule heating with a metallic microheater. **Figure 12**a,b shows a waveguide device with a lateral microheater optimized with two metals to reduce the energy consumption.[90] The optical power variation for TM polarization as a function of the applied electric power is depicted in Figure 12c. The optical loss significantly increases when the VO_2 is switched to the metallic state. Optical switching between the two optical states was carried out by applying short electrical pulses while using a static electrical power of around 25 mW. Switching energies between 200 and 300 nJ and switching speeds around 3–4 μs were reported for this kind of heater-based device.[91]

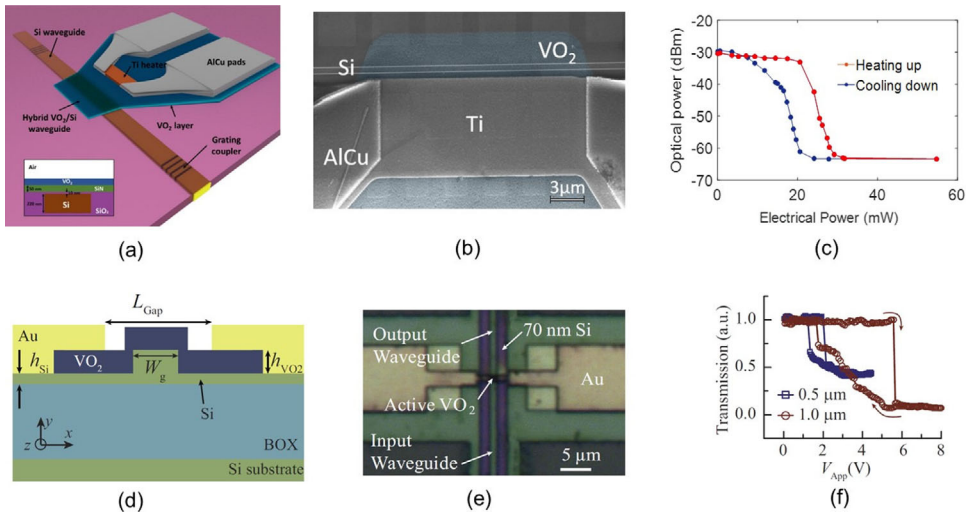

Figure 12. a) Hybrid VO_2/Si waveguide controlled by a lateral microheater, b) SEM image of the active region, and c) measured optical power variation as a function of the applied electrical power to the heater. Reproduced with permission.[90] Copyright 2018, The Optical Society. d) Hybrid VO_2/Si waveguide controlled by electrical gating, e) optical image of the fabricated device, and f) measured optical power variation as a function of the applied voltage to the electrodes. Reproduced with permission.[94] Copyright 2015, The Optical Society.

However, the physics across the VO_2 phase transition is complex, and it has been the subject of intense research. Intermediate metastable states and interplayed electronic and structural material aspects are involved.[87] In such a way, one of the main open questions is how to control them for enabling a nonvolatile optical switching performance with fast speed operation. In comparison with the heat-driven devices, an electric field gating approach has been demonstrated to reach lower consumptions (few nJ) and faster switching speeds (down to ≈1 ns) but at the expense of higher optical losses and lower extinction ratios.[94,95] Figure 12d,e shows an electrical gated hybrid VO_2/Si waveguide device and Figure 12f the measured optical transmission versus applied voltage for different lengths.[94] The switching response is volatile. However, electrical gating with a nonvolatile response has been demonstrated by including an ionic material like an electrolyte between the VO_2 and the electrode.[96,97] The electrolyte is used to inject/extract ions from the VO_2, resulting in a stabilization of the VO_2 phase transition at room temperature. Yet, the experimental demonstration of such an approach in a waveguide structure has not been reported and is still an open challenge.

On the other hand, optical excitation has been proved as the fastest way to induce the VO_2 phase transition with timescales in the femtosecond range[98–100] that would open a path to develop ultrafast all-optical bistable devices. However, until now, switching times from several seconds to hundreds of picoseconds have been achieved for hybrid photonic waveguide devices driven by optical pumping.[93,101–104] Only very recently, sub-ps switching times with switching energies between 6 and 360 nJ have been reported for a hybrid VO_2/Si photonic waveguide with out-of-plane optical pumping.[105] Therefore, a photothermal mechanism is still mostly dominant, and the difference in the timescales may be explained by the different characteristics of the control light source and the size of the VO_2 patch. Furthermore, the all-optical switching response remains volatile. Further work is required for elucidating if ultrafast switching speeds down to the femtosecond are really feasible on integrated waveguide devices and nonvolatility could be enabled. In the latter, the two main research directions are the reduction of the transition temperature by doping the VO_2 layer[106–108] or the control and stabilization of intermediate states by strain.[109,110]

4.3. Ferroelectrics

The use of ferroelectric materials such as lithium niobate,[111] barium titanate (BTO),[112] or lead zirconate titanate (PZT)[113] on various PIC platforms has generated intense research activities mostly owing to the demand of high-performance modulators for datacom applications. The key feature of ferroelectrics is their Pockels effects which enable electro-optical phase switching at ultrafast speeds without an optical loss variation. Furthermore, a hysteretic response in the variation of the relative permittivity (refractive index) can be achieved by exploiting the ferroelectric domain structure and the change of the Pockels coefficients depending on such domain structure. The hysteretic curve has typically a butterfly shape, as depicted in the upper plot of **Figure 13**a, that depends on the poling process of the ferroelectric domains and the coercive electric field of material. Yet, a nonvolatile switching performance can be achieved by shifting the hysteric curve, as seen in the lower plot of Figure 13a, by means of a permanent internal electric field induced across the ferroelectric film.[114]

Among the ferroelectric materials, BTO exhibits one of the largest Pockels coefficients, and a value as high as 923 pm V^{-1} has been demonstrated in hybrid BTO/Si waveguide devices (Figure 13b).[112] The measured hysteresis in the electro-optical phase response in a similar BTO/Si waveguide is depicted in Figure 13c.[115] The hysteresis originates from the ferroelectric domain switching driven by the electric field applied across the BTO layer, as described in the schematics below. Furthermore, the preservation of the hysteresis has been proved at fast speeds (RF frequencies up to 60 GHz)[112] and, more recently, even at cryogenic temperatures (4 K), which could find application for

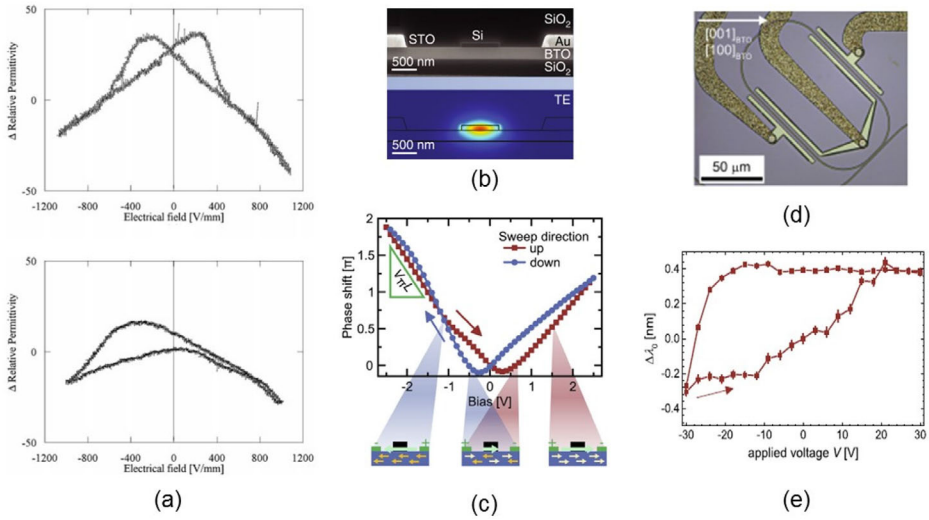

Figure 13. a) Butterfly-shaped variation of the relative permittivity at a wavelength of 633 nm with the applied electric field in the ferroelectric material of PLZT (lead lanthanum zirconate titanate). In the lower plot, the response is shifted by inducing an internal electrical field for enabling nonvolatility. Reproduced with permission.[114] Copyright 2008, The Japan Society of Applied Physics. b) Hybrid BTO/Si waveguide and optical mode for TE polarization. Reproduced under the terms of a CC-BY 4.0 license.[112] Copyright 2019, The Authors. Published by Springer Nature. c)Measured hysteresis in the electro-optical phase response around 1550 nm in a similar BTO/Si waveguide. Reproduced with permission.[115] Copyright 2019, IEEE. The schematics below describe the ferroelectric domain switching under the influence of the applied voltage. d) Ring resonator based on a hybrid BTO/Si waveguide and e) nonvolatility observed in the wavelength shift variation versus applied voltage. Reproduced with permission.[116] Copyright 2016, IEEE.

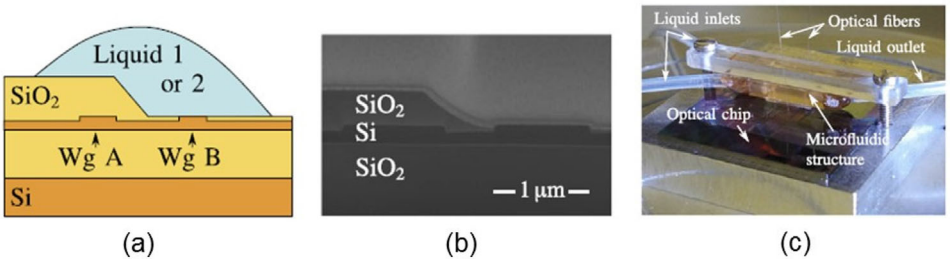

Figure 14. a) Cross section of a liquid-controlled switch device based on a directional coupler and b) SEM image of the fabricated device. c) Required microfluidic system to guide the liquid onto the chip. Reproduced with permission.[121] Copyright 2017, IEEE.

quantum photonics.[117] Nevertheless, the key challenge for enabling a nonvolatile switching is that the best approach to induce the internal electric field to shift the hysteretic response is still unknown and will depend on the ferroelectric material and waveguide structure. For instance, a nonvolatile electro-optical response was observed in a ring resonator based on a hybrid BTO/Si waveguide (Figure 13d).[116] Figure 13e shows the wavelength shift of the resonance as a function of the applied voltage. The origin of the nonvolatility was attributed to an internal electric field induced by redistribution of free charges at the layer interfaces. On the other hand, stability over time is also a major challenge (see supplement of ref. [112]). Recently, multistate electro-optical switching has been reported but with retention times of only 6 min.[118]

4.4. Liquids

The use of liquids on silicon photonic devices has also been proposed and demonstrated for enabling nonvolatile photonic switching with an optical broadband operation.[119,120] The switching performance relies on electrowetting actuation, which allows two liquids exhibiting different refractive indices to be moved and deposited on top of a photonic device. Nonvolatility stems from the remaining liquid when the actuation voltage is removed. Optical switching has been achieved by using a liquid-controlled switch device based on a directional coupler.[121] The cross section of the coupler and a scanning electron microscopy (SEM) image of the fabricated device are shown in **Figure 14**a,b. The oxide cladding lying on top of one of the coupler waveguides is locally removed to maximize the overlap between the optical mode and the liquid. The refractive indices of the two liquids were 1.43 and 1.63 for providing a large enough index difference. However, even so, long switching lengths of 0.6 and 1.4 mm were required following an adiabatic design for achieving a broadband operation with an extinction ratio above 11 and 38 dB, respectively.

An additional experiment was reported to improve the switch performance via substituting the high-index liquid by air to achieve a larger refractive index change. As a result, the extinction ratio was improved above 20 dB for the shortest length,

Table 1. Qualitative comparison of the approaches for enabling nonvolatile photonic switching in silicon-based devices.

Approach	Phase actuator	Intensity actuator	Excitation	Switching energy	Switching speed	Footprint	Manufacturing process
GST/Si	–	++	O/E	+	+	++	++
Flash memory	+	+	E	+	–	+	++
Resistive switching	–	++	E	++	+	++	+
Liquid/Si	++	–	E	+	–	–	+

Note: ++ Excellent; + Medium;– Limited; O/E Optical/Electrical.

although the use of air instead of liquid increased the actuation voltage. On the other hand, insertion losses below 1 dB were reported, while a value lower than 0.02 dB was predicted to be achievable through design optimizations. A 16 × 16 switching matrix based on the liquid-controlled coupler switch has also been successfully demonstrated.[122] However, the required voltages or switching energies have not been provided, and switching times are limited to the millisecond range. Furthermore, a microfluidic system is required to guide the liquid onto the chip, as depicted in Figure 14c. The long-term stability and potential switching degradation at high temperatures also remain as open challenges.

5. Conclusions and Perspectives

Optical bistability with ultralow holding power can be simply achieved in silicon by using a photonic structure that provides optical feedback. However, nonvolatility is not possible because the optical bistability is driven by the optical power of the pumping signal. Thereby, several and diverse approaches have been proposed for enabling nonvolatile photonic switching in silicon waveguide devices.

Table 1 summarizes the main approaches where nonvolatile switching has been demonstrated in silicon waveguide devices. Nowadays, the dominant approach is based on the integration of GST which provides a large and nonvolatile multilevel change on its refractive index at room temperature that gives rise to ultracompact devices. However, GST exhibits a rather high optical absorption at telecom wavelengths, which makes it difficult to induce phase shifts with low optical loss. Hence, although GST has been mostly proved for optical memory cells, it is not the best candidate for phase actuators. Other chalcogenides such as GSST may provide lower optical losses but experimental demonstrations are needed. On the other hand, the temperature-driven switching process limits the switching speed and energy. Switching speeds in the nanosecond range and switching energies around few nanojoules have been typically demonstrated in GST/Si waveguides with a few micrometers length and triggered by both optical and electrical excitations. Nevertheless, a switching energy as small as 16 pJ has been recently demonstrated by using plasmonic waveguide structures but at expense of a low extinction ratio (<1 dB).[80]

Electronic approaches could be used to remove the temperature mechanism. In this way, flash-like devices may be an option. One of the main advantages is that the fabrication is based on standard CMOS process steps. However, current experimental demonstrations rely on the weak plasma-dispersion effect of silicon and show slow switching speeds and high driving voltages. A switching time of 600 ms with voltages up to 20 V has been required for achieving extinction ratios above 20 dB in a ring device.[25] Larger phase shifts and absorption changes are predicted by using alternative materials with superior properties, such as graphene or ITO. Yet, although several works have shown promising results, there is no experimental demonstration to date. On the other hand, resistive switching is another alternative to achieve ultracompact footprints, fast switching, and low driving voltages but only for intensity actuators. However, this research field is still incipient, with only few demonstrations with relatively large insertion losses and many open questions about the optimal active materials and waveguide structure as well as control of the underlying physics to ensure reproducibility. Switching energies as low as 12.5 fJ with an extinction ratio up to 9.2 dB have been demonstrated but with a nonvolatile plasmonic device and switching speeds in the microsecond range.[41]

Following a different approach, liquid/Si devices have been developed for providing a nonvolatile phase shift with low optical losses and without the need of extra processing steps. In this case, switching speeds are slower (in the millisecond range) owing to the underlying actuation mechanism and its utilization may be restricted owing to the necessity of a microfluidic system. However, high extinction ratios above 20 dB with insertion losses below 1 dB have been demonstrated by means of a directional coupler device.[122]

Table 2 summarizes the solutions for optical switching with bistability but where nonvolatility is still under progress. Silicon MEMS devices have emerged in the past year as a strong solution for implementing photonic switching devices. The mechanical displacement of photonic waveguides allows to obtain very low insertion losses (<0.5 dB) and ultralarge extinction ratio (>60 dB) with switching times of 300 ns.[55] Long-term stability and high scalability have also been demonstrated. However, nonvolatility still needs development, large footprints are required, and the fabrication process requires additional steps that increase the complexity and cost of the final device. On the other hand, VO_2 could be an alternative material for GST by providing also a large optical contrast but with faster speeds and lower switching energies. This could allow optical memory cells of a few micrometers long with switching times potentially in the femtosecond range. Very recently, sub-picosecond switching times with switching energies down to 6 nJ have been demonstrated for VO_2/Si photonic waveguides by using out-of-plane optical excitation.[105] However, the material change is volatile, and the strategies for enabling a nonvolatility switching performance have not yet

Table 2. Qualitative comparison of the approaches for enabling optical bistable switching in silicon devices but where nonvolatility is still under progress.

Approach	Phase actuator	Intensity actuator	Excitation	Switching energy	Switching speed	Footprint	Manufacturing process
MEMS	++	++	E	+	+	−	+
VO_2/Si	−	++	O/E	+	++	++	++
Ferroelectrics/Si	++	−	E	++	++	+	+

Note: ++ Excellent; + Medium; − Limited; O/E Optical/Electrical.

been demonstrated in waveguide devices. In addition, VO_2 is also not favorable for developing phase actuators owing to the large optical loss in the metallic state.

A wide range of applications ranging from programmable photonics and LIDAR systems to neuromorphic computing could benefit from nonvolatile phase actuators. Ferroelectrics provide an optical phase shift without loss variation, owing to the electro-optical Pockels effect, together with fast speeds and ultralow energy consumption. Among them, BTO stands out as an excellent choice owing to its high Pockels coefficient and CMOS compatibility. Switching speeds in the picosecond range have been demonstrated in BTO/Si devices with an estimated switching energy as low as 96 fJ.[112] However, the optimal route for enabling a reproducible and long-term nonvolatile switching performance has not yet been demonstrated.

In conclusion, to date, the optimal nonvolatile approach will be probably different depending on the target application. On the one hand, the best performance metrics, such as switching energy, speed, extinction ratio, or insertion losses show tradeoffs among the different proposed approaches. Nonvolatile intensity actuators with high performance have been demonstrated, however, the best option for enabling nonvolatile phase actuators is still an open issue. On the other hand, the integration into the silicon photonics platform with the lowest complexity and high scalability might be an important requirement. In addition, critical issues such as the long-term stability or retention times have not been demonstrated in most of the devices reported so far. Nevertheless, despite all these challenges, it seems clear that nonvolatile elements will be progressively integrated on the silicon platform in the next years. We expect that this review will stimulate future research and development endeavors in this promising field and open up new ways for enabling nonvolatility.

Acknowledgements

This work was supported by Ministerio de Economia y Competitividad (MINECO) (TEC2016-76849); Ministerio de Ciencia e Innovacion (PID2019-111460GB-I00, FPU17/04224); and Generalitat Valenciana (PROMETEO/2019/123).

Conflict of Interest

The authors declare no conflict of interest.

Keywords

nonvolatile, optical switching, photonic integrated circuits, photonic memory, photonic waveguides, silicon photonics

Received: November 12, 2020
Revised: March 11, 2021
Published online: May 5, 2021

[1] X. Chen, M. M. Milosevic, S. Stanković, S. Reynolds, T. D. Bucio, K. Li, D. J. Thomson, F. Gardes, G. T. Reed, *Proc. IEEE* **2018**, *106*, 2101.
[2] A. Rahim, T. Spuesens, R. Baets, W. Bogaerts, *Proc. IEEE* **2018**, *106*, 2313.
[3] A. H. Atabaki, S. Moazeni, F. Pavanello, H. Gevorgyan, J. Notaros, L. Alloatti, M. T. Wade, C. Sun, S. A. Kruger, H. Meng, K. Al Qubaisi, I. Wang, B. Zhang, A. Khilo, C. V. Baiocco, M. A. Popović, V. M. Stojanović, R. J. Ram, *Nature* **2018**, *556*, 349.
[4] W. Bogaerts, L. Chrostowski, *Laser Photonics Rev.* **2018**, *12*, 1.
[5] W. Bogaerts, D. Pérez, J. Capmany, D. A. B. Miller, J. Poon, D. Englund, F. Morichetti, A. Melloni, *Nature* **2020**, *586*, 207.
[6] R. Soref, *APL Photonics* **2018**, *3*, 021101.
[7] Q. Cheng, S. Rumley, M. Bahadori, K. Bergman, *Opt. Express* **2018**, *26*, 16022.
[8] T. Alexoudi, G. T. Kanellos, N. Pleros, *Light: Sci. Appl.* **2020**.
[9] Y. Zhai, J. Q. Yang, Y. Zhou, J. Y. Mao, Y. Ren, V. A. L. Roy, S. T. Han, *Mater. Horiz.* **2018**, *5*, 641.
[10] T. Ferreira De Lima, B. J. Shastri, A. N. Tait, M. A. Nahmias, P. R. Prucnal, *Nanophotonics* **2017**, *6*, 577.
[11] J. Sun, E. Timurdogan, A. Yaacobi, E. S. Hosseini, M. R. Watts, *Nature* **2013**, *493*, 195.
[12] X. Sun, L. Zhang, Q. Zhang, W. Zhang, *Appl. Sci.* **2019**, *9*, 4225.
[13] C. V. Poulton, M. J. Byrd, P. Russo, E. Timurdogan, M. Khandaker, D. Vermeulen, M. R. Watts, *IEEE J. Sel. Top. Quantum Electron.* **2019**, *25*, 1.
[14] V. R. Almeida, M. Lipson, *Opt. Lett.* **2004**, *29*, 2387.
[15] G. Priem, P. Dumon, W. Bogaerts, D. Van Thourhout, G. Morthier, R. Baets, *Opt. Express* **2005**, *13*, 9623.
[16] P. E. Barclay, K. Srinivasan, O. Painter, *Opt. Express* **2005**, *13*, 801.
[17] X. Zheng, Y. Luo, G. Li, I. Shubin, H. Thacker, J. Yao, K. Raj, J. E. Cunningham, A. V. Krishnamoorthy, *Opt. Express* **2012**, *20*, 11478.
[18] M. Notomi, A. Shinya, S. Mitsugi, G. Kira, E. Kuramochi, T. Tanabe, *Opt. Express* **2005**, *13*, 2678.
[19] Q. Xu, M. Lipson, *Opt. Lett.* **2006**, *31*, 341.
[20] L.-W. Luo, G. S. Wiederhecker, K. Preston, M. Lipson, *Opt. Lett.* **2012**, *37*, 590.
[21] T. Tanabe, M. Notomi, S. Mitsugi, A. Shinya, E. Kuramochi, *Opt. Lett.* **2005**, *30*, 2575.
[22] E. Kuramochi, K. Nozaki, A. Shinya, K. Takeda, T. Sato, S. Matsuo, H. Taniyama, H. Sumikura, M. Notomi, *Nat. Photonics* **2014**, *8*, 474.
[23] A. Majumdar, A. Rundquist, *Opt. Lett.* **2014**, *39*, 3864.
[24] Y.-S. Shen, K.-Y. Chen, P.-C. Chen, T.-C. Chen, Y.-H. Wu, *Sci. Rep.* **2017**, *7*, 43659.
[25] J. F. Song, X. S. Luo, A. E. J. Lim, C. Li, Q. Fang, T. Y. Liow, L. X. Jia, X. G. Tu, Y. Huang, H. F. Zhou, G. Q. Lo, *Sci. Rep.* **2016**, *6*, 22616.
[26] C. A. Barrios, M. Lipson, *J. Light Technol* **2006**, *24*, 2898.

[27] M. Grajower, N. Mazurski, J. Shappir, U. Levy, *Laser Photonics Rev.* **2018**, *12*, 1700190.
[28] J.-F. Song, A. E.-J. Lim, X.-S. Luo, Q. Fang, C. Li, L. X. Jia, X.-G. Tu, Y. Huang, H.-F. Zhou, T.-Y. Liow, G.-Q. Lo, *Opt. Express* **2016**, *24*, 21744.
[29] I. Olivares, J. Parra, P. Sanchis, *IEEE Photonics J.* **2021**, *13*, 4600108.
[30] Y. Li, W. Chen, T. Dai, P. Wang, *Appl. Phys. Express* **2019**, *12*, 102005.
[31] Z. Ma, Z. Li, K. Liu, C. Ye, V. J. Sorger, *Nanophotonics* **2015**, *4*, 198.
[32] J. Parra, I. Olivares, A. Brimont, P. Sanchis, *Opt. Lett.* **2019**, *44*, 3932.
[33] J. Parra, I. Olivares, A. Brimont, P. Sanchis, presented at 2019 IEEE 16th Int. Conf. Group IV Photonics, Malaga, Spain, August **2019**.
[34] J. Parra, I. Olivares, F. Ramos, P. S. Kilders, *Opt. Lett.* **2020**, *45*, 1503.
[35] B. Hwang, J. S. Lee, *Adv. Electron. Mater.* **2019**, *5*, 1800519.
[36] Z. Wang, H. Wu, G. W. Burr, C. S. Hwang, K. L. Wang, Q. Xia, J. J. Yang, *Nat. Rev. Mater.* **2020**, *5*, 173.
[37] R. Waser, M. Aono, *Nat. Mater.* **2007**, *6*, 833.
[38] H. Wang, X. Yan, *Phys. Status Solidi RRL* **2019**, *13*, 1900073.
[39] U. Koch, C. Hoessbacher, A. Emboras, J. Leuthold, *J. Electroceram.* **2017**, *39*, 239.
[40] A. Emboras, I. Goykhman, B. Desiatov, N. Mazurski, L. Stern, J. Shappir, U. Levy, *Nano Lett.* **2013**, *13*, 6151.
[41] A. Emboras, J. Niegemann, P. Ma, C. Haffner, A. Pedersen, M. Luisier, C. Hafner, T. Schimmel, J. Leuthold, *Nano Lett.* **2016**, *16*, 709.
[42] C. Hoessbacher, Y. Fedoryshyn, A. Emboras, A. Melikyan, M. Kohl, D. Hillerkuss, C. Hafner, J. Leuthold, *Optica* **2014**, *1*, 198.
[43] G. Vescio, A. Crespo-Yepes, D. Alonso, S. Claramunt, M. Porti, R. Rodriguez, A. Cornet, A. Cirera, M. Nafria, X. Aymerich, *IEEE Electron Device Lett.* **2017**, *38*, 457.
[44] J. J. Yang, F. Miao, M. D. Pickett, D. A. A. Ohlberg, D. R. Stewart, C. N. Lau, R. S. Williams, *Nanotechnology* **2010**, *21*, 215201.
[45] O. Blázquez, J. L. Frieiro, J. López-Vidrier, C. Guillaume, X. Portier, C. Labbé, P. Sanchis, S. Hernández, B. Garrido, *Appl. Phys. Lett.* **2018**, *113*, 183502.
[46] A. Mehonic, S. Cueff, M. Wojdak, S. Hudziak, C. Labbé, R. Rizk, A. J. Kenyon, *Nanotechnology* **2012**, *23*, 455201.
[47] M. Wojdak, S. Hudziak, O. Jambois, B. Garrido, R. Rizk, A. J. Kenyon, *J. Appl. Phys.* **2012**, *111*, 074507.
[48] Y. Yang, P. Gao, S. Gaba, T. Chang, X. Pan, W. Lu, *Nat. Commun.* **2012**, *3*, 732.
[49] E. Battal, A. Ozcan, A. K. Okyay, *Adv. Opt. Mater.* **2014**, *2*, 1149.
[50] W. Noell, P. A. Clerc, L. Dellmann, B. Guldimann, H. P. Herzig, O. Manzardo, C. R. Marxer, K. J. Weible, R. Dändliker, N. De Rooij, *IEEE J. Sel. Top. Quantum Electron.* **2002**, *8*, 148.
[51] C. Errando-Herranz, A. Y. Takabayashi, P. Edinger, H. Sattari, K. B. Gylfason, N. Quack, *IEEE J. Sel. Top. Quantum Electron.* **2020**, *26*, 1.
[52] E. Bulgan, Y. Kanamori, K. Hane, *Appl. Phys. Lett.* **2008**, *92*, 101110.
[53] H. B. Liu, F. Chollet, *J. Microelectromech. Syst.* **2009**, *18*, 715.
[54] H. Sattari, A. Toros, T. Graziosi, N. Quack, in *MOEMS Miniaturized Systems XVIII* (Eds: W. Piyawattanametha, Y.-H. Park, H. Zappe), SPIE, Bellingham, WA **2019**, p. 13.
[55] T. J. Seok, N. Quack, S. Han, R. S. Muller, M. C. Wu, *Optica* **2016**, *3*, 64.
[56] T. J. Seok, K. Kwon, J. Henriksson, J. Luo, M. C. Wu, *Optica* **2019**, *6*, 490.
[57] M. Wuttig, N. Yamada, *Nat. Mater.* **2007**, *6*, 824.
[58] W. H. P. Pernice, H. Bhaskaran, *Appl. Phys. Lett.* **2012**, *101*, 171101.
[59] M. Wuttig, H. Bhaskaran, T. Taubner, *Nat. Photonics* **2017**, *11*, 465.
[60] S. Abdollahramezani, O. Hemmatyar, H. Taghinejad, A. Krasnok, Y. Kiarashinejad, M. Zandehshahvar, A. Alù, A. Adibi, *Nanophotonics* **2020**, *9*, 1189.
[61] K. Shportko, S. Kremers, M. Woda, D. Lencer, J. Robertson, M. Wuttig, *Nat. Mater.* **2008**, *7*, 653.
[62] Y. Zhang, J. B. Chou, J. Li, H. Li, Q. Du, A. Yadav, S. Zhou, M. Y. Shalaginov, Z. Fang, H. Zhong, C. Roberts, P. Robinson, B. Bohlin, C. Ríos, H. Lin, M. Kang, T. Gu, J. Warner, V. Liberman, K. Richardson, J. Hu, *Nat. Commun.* **2019**, *10*, 4279.
[63] M. Stegmaier, C. RÍos, H. Bhaskaran, W. H. P. Pernice, *ACS Photonics* **2016**, *3*, 828.
[64] E. Gemo, S. V. Kesava, C. Ruiz De Galarreta, L. Trimby, S. G.-C. Carrillo, M. Riede, A. Baldycheva, A. Alexeev, C. D. Wright, *Opt. Mater. Express* **2020**, *10*, 1675.
[65] H. Zhang, L. Zhou, J. Xu, L. Lu, J. Chen, B. M. A. Rahman, *Opt. Lett.* **2018**, *43*, 5539.
[66] D. Tanaka, Y. Shoji, M. Kuwahara, X. Wang, K. Kintaka, H. Kawashima, T. Toyosaki, Y. Ikuma, H. Tsuda, *Opt. Express* **2012**, *20*, 10283.
[67] J. Zheng, A. Khanolkar, P. Xu, S. Colburn, S. Deshmukh, J. Myers, J. Frantz, E. Pop, J. Hendrickson, J. Doylend, N. Boechler, A. Majumdar, *Opt. Mater. Express* **2018**, *8*, 1551.
[68] D. Loke, T. H. Lee, W. J. Wang, L. P. Shi, R. Zhao, Y. C. Yeo, T. C. Chong, S. R. Elliott, *Science* **2012**, *336*, 1566.
[69] Y. Ikuma, Y. Shoji, M. Kuwahara, X. Wang, K. Kintaka, H. Kawashima, D. Tanaka, H. Tsuda, *Electron. Lett.* **2010**, *46*, 368.
[70] M. Rudé, J. Pello, R. E. Simpson, J. Osmond, G. Roelkens, J. J. G. M. van der Tol, V. Pruneri, *Appl. Phys. Lett.* **2013**, *103*, 141119.
[71] C. Ríos, N. Youngblood, Z. Cheng, M. Le Gallo, W. H. P. Pernice, C. D. Wright, A. Sebastian, H. Bhaskaran, *Sci. Adv.* **2019**, *5*, eaau5759.
[72] C. Rios, M. Stegmaier, P. Hosseini, D. Wang, T. Scherer, C. D. Wright, H. Bhaskaran, W. H. P. Pernice, *Nat. Photonics* **2015**, *9*, 725.
[73] C. Rios, M. Stegmaier, Z. Cheng, N. Youngblood, C. D. Wright, W. H. P. Pernice, H. Bhaskaran, *Opt. Mater. Express* **2018**, *8*, 2455.
[74] X. Li, N. Youngblood, C. Ríos, Z. Cheng, C. D. Wright, W. H. Pernice, H. Bhaskaran, *Optica* **2019**, *6*, 1.
[75] X. Li, N. Youngblood, Z. Cheng, S. G.-C. Carrillo, E. Gemo, W. H. P. Pernice, C. D. Wright, H. Bhaskaran, *Optica* **2020**, *7*, 218.
[76] K. Kato, M. Kuwahara, H. Kawashima, T. Tsuruoka, H. Tsuda, *Appl. Phys. Express* **2017**, *10*, 072201.
[77] J. Parra, J. Hurtado, A. Griol, P. Sanchis, *Opt. Express* **2020**, *28*, 9393.
[78] H. Zhang, L. Zhou, J. Xu, N. Wang, H. Hu, L. Lu, B. M. A. Rahman, J. Chen, *Sci. Bull.* **2019**, *64*, 782.
[79] H. Zhang, L. Zhou, L. Lu, J. Xu, N. Wang, H. Hu, B. M. A. Rahman, Z. Zhou, J. Chen, *ACS Photonics* **2019**, *6*, 2205.
[80] N. Farmakidis, N. Youngblood, X. Li, J. Tan, J. L. Swett, Z. Cheng, C. D. Wright, W. H. P. Pernice, H. Bhaskaran, *Sci. Adv.* **2019**, *5*, eaaw2687.
[81] C. Wu, H. Yu, H. Li, X. Zhang, I. Takeuchi, M. Li, *ACS Photonics* **2019**, *6*, 87.
[82] M. Miscuglio, J. Meng, O. Yesiliurt, Y. Zhang, L. J. Prokopeva, A. Mehrabian, J. Hu, A. V. Kildishev, V. J. Sorger, in *Conf. Lasers Electro-Optics*, OSA, Washington, DC **2020**, p. JF3A.2.
[83] Q. Zhang, Y. Zhang, J. Li, R. Soref, T. Gu, J. Hu, *Opt. Lett.* **2018**, *43*, 94.
[84] W. Jiang, *Sci. Rep.* **2018**, *8*, 15946.
[85] M. Miscuglio, V. J. Sorger, *Appl. Phys. Rev.* **2020**, *7*, 031404.
[86] Z. Shao, X. Cao, H. Luo, P. Jin, *NPG Asia Mater.* **2018**, *10*, 581.
[87] S. Cueff, J. John, Z. Zhang, J. Parra, J. Sun, R. Orobtchouk, S. Ramanathan, P. Sanchis, *APL Photonics* **2020**, *5*, 110901.
[88] R. M. Briggs, I. M. Pryce, H. A. Atwater, *Opt. Express* **2010**, *18*, 11192.
[89] M. Currie, M. A. Mastro, V. D. Wheeler, *Opt. Mater. Express* **2017**, *7*, 1697.
[90] I. Olivares, L. Sánchez, J. Parra, R. Larrea, A. Griol, M. Menghini, P. Homm, L.-W. Jang, B. van Bilzen, J. W. Seo, J.-P. Locquet, P. Sanchis, *Opt. Express* **2018**, *26*, 12387.
[91] L. D. Sánchez, I. Olivares, J. Parra, M. Menghini, P. Homm, J.-P. Locquet, P. Sanchis, *Opt. Lett.* **2018**, *43*, 3650.

[92] V. Jeyaselvan, A. Pal, P. S. A. Kumar, S. K. Selvaraja, *OSA Continuum* **2020**, *3*, 132.
[93] J. Parra, T. Ivanova, M. Menghini, P. Homm, J.-P. Locquet, P. Sanchiskilders, *J. Light Technol.* **2021**.
[94] A. Joushaghani, J. Jeong, S. Paradis, D. Alain, J. Stewart Aitchison, J. K. S. Poon, *Opt. Express* **2015**, *23*, 3657.
[95] P. Markov, R. E. Marvel, H. J. Conley, K. J. Miller, R. F. Haglund, S. M. Weiss, *ACS Photonics* **2015**, *2*, 1175.
[96] S. Chen, Z. Wang, H. Ren, Y. Chen, W. Yan, C. Wang, B. Li, J. Jiang, C. Zou, *Sci. Adv.* **2019**, *5*, eaav6815.
[97] K. Liu, D. Fu, J. Cao, J. Suh, K. X. Wang, C. Cheng, D. F. Ogletree, H. Guo, S. Sengupta, A. Khan, C. W. Yeung, S. Salahuddin, M. M. Deshmukh, J. Wu, *Nano Lett.* **2012**, *12*, 6272.
[98] A. Cavalleri, C. Tóth, C. W. Siders, J. A. Squier, F. Ráksi, P. Forget, J. C. Kieffer, *Phys. Rev. Lett.* **2001**, *87*, 237401.
[99] A. Cavalleri, T. Dekorsy, H. H. W. Chong, J. C. Kieffer, R. W. Schoenlein, *Phys. Rev. B* **2004**, *70*, 161102.
[100] M. R. Otto, L. P. René de Cotret, D. A. Valverde-Chavez, K. L. Tiwari, N. Émond, M. Chaker, D. G. Cooke, B. J. Siwick, *Proc. Natl. Acad. Sci. USA* **2019**, *116*, 450.
[101] J. D. Ryckman, V. Diez-Blanco, J. Nag, R. E. Marvel, B. K. Choi, R. F. Haglund, S. M. Weiss, *Opt. Express* **2012**, *20*, 13215.
[102] J. D. Ryckman, K. A. Hallman, R. E. Marvel, R. F. Haglund, S. M. Weiss, *Opt. Express* **2013**, *21*, 10753.
[103] H. M. K. Wong, Z. Yan, K. A. Hallman, R. E. Marvel, R. P. Prasankumar, R. F. Haglund, A. S. Helmy, *ACS Photonics* **2019**, *6*, 2734.
[104] K. Shibuya, K. Ishii, Y. Atsumi, T. Yoshida, Y. Sakakibara, M. Mori, A. Sawa, *Opt. Express* **2020**, *28*, 37188.
[105] K. A. Hallman, K. J. Miller, A. Baydin, S. M. Weiss, R. F. Haglund, *Adv. Opt. Mater.* **2020**, *8*, 2001721.
[106] X. Tan, T. Yao, R. Long, Z. Sun, Y. Feng, H. Cheng, X. Yuan, W. Zhang, Q. Liu, C. Wu, Y. Xie, S. Wei, *Sci. Rep.* **2012**, *2*, 466.
[107] Y. Zhao, G. Karaoglan-Bebek, X. Pan, M. Holtz, A. A. Bernussi, Z. Fan, *Appl. Phys. Lett.* **2014**, *104*, 241901.
[108] N. R. Mlyuka, G. A. Niklasson, C. G. Granqvist, *Appl. Phys. Lett.* **2009**, *95*, 171909.
[109] J. Laverock, S. Kittiwatanakul, A. Zakharov, Y. Niu, B. Chen, S. A. Wolf, J. W. Lu, K. E. Smith, *Phys. Rev. Lett.* **2014**, *113*, 216402.
[110] N. F. Quackenbush, H. Paik, M. J. Wahila, S. Sallis, M. E. Holtz, X. Huang, A. Ganose, B. J. Morgan, D. O. Scanlon, Y. Gu, F. Xue, L. Q. Chen, G. E. Sterbinsky, C. Schlueter, T. L. Lee, J. C. Woicik, J. H. Guo, J. D. Brock, D. A. Muller, D. A. Arena, D. G. Schlom, L. F. J. Piper, *Phys. Rev. B* **2016**, *94*, 085105.
[111] Y. Qi, Y. Li, *Nanophotonics* **2020**, *9*, 1287.
[112] S. Abel, F. Eltes, J. E. Ortmann, A. Messner, P. Castera, T. Wagner, D. Urbonas, A. Rosa, A. M. Gutierrez, D. Tulli, P. Ma, B. Baeuerle, A. Josten, W. Heni, D. Caimi, L. Czornomaz, A. A. Demkov, J. Leuthold, P. Sanchis, J. Fompeyrine, *Nat. Mater.* **2019**, *18*, 42.
[113] K. Alexander, J. P. George, J. Verbist, K. Neyts, B. Kuyken, D. Van Thourhout, J. Beeckman, *Nat. Commun.* **2018**, *9*, 3444.
[114] T. Ohashi, H. Hosaka, T. Morita, *Jpn. J. Appl. Phys.* **2008**, *47*, 3985.
[115] F. Eltes, C. Mai, D. Caimi, M. Kroh, Y. Popoff, G. Winzer, D. Petousi, S. Lischke, J. E. Ortmann, L. Czornomaz, L. Zimmermann, J. Fompeyrine, S. Abel, *J. Light Technol.* **2019**, *37*, 1456.
[116] S. Abel, T. Stöferle, C. Marchiori, D. Caimi, L. Czornomaz, M. Stuckelberger, M. Sousa, B. J. Offrein, J. Fompeyrine, *J. Light Technol.* **2016**, *34*, 1688.
[117] F. Eltes, G. E. Villarreal-Garcia, D. Caimi, H. Siegwart, A. A. Gentile, A. Hart, P. Stark, G. D. Marshall, M. G. Thompson, J. Barreto, J. Fompeyrine, S. Abel, *Nat. Mater.* **2020**, *19*, 1164.
[118] P. Stark, J. G. Kremer, F. Eltes, D. Caimi, J. Fompeyrine, B. J. Offrein, S. Abel, in *2019 Conf. Lasers Electro-Optics Europe & European Quantum Electronics Conf.*, IEEE, Piscataway, NJ **2019**, p. 1.
[119] K. Nakatsuhara, A. Kato, Y. Hayama, *Opt. Express* **2014**, *22*, 9597.
[120] S. Gunther, C. Endrödy, S. Si, S. Weinberger, R. Claes, Y. Justo, H. D'Heer, A. Neft, M. Hoffmann, *Proc. IEEE Int. Conf. Micro Electro Mech. Syst.* **2017**, 1329.
[121] H. Dheer, C. L. Arce, S. Vandewiele, J. Watte, K. Huybrechts, R. Baets, D. Van Thourhout, *J. Light Technol.* **2017**, *35*, 2948.
[122] H. D'Heer, K. Saurav, C. Lerma Arce, M. Detalle, G. Lepage, P. Verheyen, J. Watte, D. Van Thourhout, *IEEE Photonics Technol. Lett.* **2018**, *30*, 1258.

Jorge Parra received his B.Sc. and M.Sc. degrees in telecommunications engineering in 2016 and 2018, respectively, from the Universitat Politècnica de València, Spain. He is currently working towards his Ph.D. degree in telecommunication engineering at the Nanophotonics Technology Center. His research interests focus on silicon photonics, and the emerging epsilon-near-zero (ENZ) and phase change integrated photonics platforms.

Irene Olivares received her B.S. degree in physics from Complutense University, Madrid, Spain, in 2014 and the M.S. degree in renewable energies from the Complutense University, Madrid, Spain in 2015. She is pursuing the Ph.D. degree in telecommunication engineering at Politècnica University, Valencia, Spain. Her research interest includes the development and design of photonic integrated circuits and has especially worked in the topic of strained silicon. She has also been researching in the area of phase change materials.

Antoine Brimont received an Engineering Master's degree in materials science and nanotechnology from the Institut National des Sciences Appliquées de Rennes, France, as well as an MSc degree in physics in collaboration with the University of Rennes, France, in 2005. Furthermore, he received his PhD degree in telecommunication (electrical) engineering from the Universitat Politècnica de València, Spain, in 2011. He has been working for 10 years as a senior research engineer at the Valencia Nanophotonics Technology Center and he recently moved to Ligentec SA (Switzerland), a spin-off company from the Ecole Polytechnique Fédérale de Lausanne (EPFL), where he is currently fulfilling the role of senior characterisation engineer. Antoine's research interests encompass integrated silicon and silicon nitride photonics integrated circuits (PICs) for a broad range of applications (quantum computing, lidar, space and metrology and communications). He has authored or co-authored more than 70 papers in peer-reviewed international journals and international conferences.

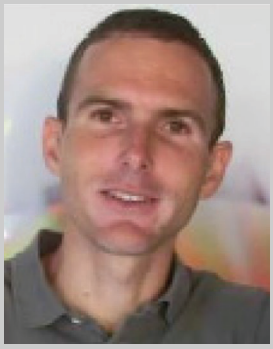

Pablo Sanchis received his PhD degree from the Universitat Politècnica de València (Spain) in 2005. He is full-professor at the same university since 2016. His research career has been developed at the Nanophotonics Technology Center where he leads a research group. His research interests are basically related with the design, fabrication and characterization of photonic integrated circuits, especially in the field of silicon photonics. He has authored more than 80 papers in peer-reviewed international journals and more than 140 papers in international conferences and he holds several patents. He has also been part of the organization committee of ECOC, ECIO, and other international conferences.